

Double charge exchange to the double isobaric analog state at $T_\pi \sim 292$ MeV

J. D. Zumbro, H. T. Fortune, and M. Burlein

University of Pennsylvania, Philadelphia, Pennsylvania 19104

C. L. Morris and Z.-F. Wang*

Los Alamos National Laboratory, Los Alamos, New Mexico 87545

R. Gilman[†]

*University of Pennsylvania, Philadelphia, Pennsylvania 19104
and Argonne National Laboratory, Argonne, Illinois 60439*

Kalvir S. Dhuga and G. R. Burleson

New Mexico State University, Las Cruces, New Mexico 88003

M. W. Rawool and R. W. Garnett

*New Mexico State University, Las Cruces, New Mexico 88003
and Argonne National Laboratory, Argonne, Illinois 60439*

M. J. Smithson, D. S. Oakley, S. Mordechai,[‡] C. Fred Moore, and M. A. Machuca

University of Texas at Austin, Austin, Texas 78712

D. L. Watson

*Los Alamos National Laboratory, Los Alamos, New Mexico 87545
and University of York, Heslington, York YO1 5DD, United Kingdom*

N. Auerbach

*Los Alamos National Laboratory, Los Alamos, New Mexico 87545
and University of Tel Aviv, Tel Aviv, Israel*

(Received 27 April 1987)

Measurements of cross sections for the (π^+, π^-) reaction to the double isobaric analog state on targets of ^{30}Si , ^{34}S , ^{44}Ca , ^{50}Ti , ^{51}V , ^{52}Cr , and ^{58}Ni at $\theta_{\text{lab}} = 5^\circ$ and an incident pion kinetic energy of ~ 292 MeV are presented. We also present limits for the cross section to the residual ground state for the four $T > 1$ targets. The data are compared with a phenomenological two-amplitude model and with a two-amplitude model that uses seniority-zero shell-model wave functions. The latter model provides expressions for both ground state and double isobaric analog state cross sections.

One of the mysteries of the (π^+, π^-) double-charge-exchange (DCX) reaction to the double isobaric analog state (DIAS) has been the apparent difference in the mass dependence of the forward angle (generally 5°) differential cross section for the reaction on $T = 1$ targets and on $T > 1$ targets. The mass dependence in general is well reproduced by an $A_{\text{tgt}}^{-10/3}$ behavior.¹ However, as first pointed out by Seidl *et al.*² and noted in Ref. 1, if only $T = 1$ targets are considered the data are reproduced by an $A_{\text{tgt}}^{-7/3}$ dependence rather than by $A_{\text{tgt}}^{-10/3}$.

Fortune and Gilman³ (hereafter referred to as FG) have applied an earlier, phenomenological, two-amplitude model^{4,5} to the DIAS data at 292 MeV. In this two-amplitude model the DCX cross section is given by

$$\frac{d\sigma^{\text{DIAS}}}{d\Omega_{\text{DCX}}} = |f_{\text{NA}} + f_{\text{DIAT}} \times e^{i\phi}|^2. \quad (1)$$

The term, f_{DIAT} , is the amplitude that proceeds through the double isobaric analog transition (DIAT) and has the expected⁶ form

$$f_{\text{DIAT}}(A_{\text{tgt}}) = \left[\frac{(N-Z)(N-Z-1)}{2} \right]^{1/2} \times \left[\frac{18}{A_{\text{tgt}}} \right]^{5/3} f_{\text{DIAT}}(^{18}\text{O}). \quad (2)$$

The term, f_{NA} , is a nonanalog amplitude and is assumed to vary as

$$f_{\text{NA}}(A_{\text{tgt}}) = \left[\frac{16}{A_{\text{core}}} \right]^{2/3} f_{\text{NA}}(^{18}\text{O}). \quad (3)$$

The relative phase between the two amplitudes is ϕ . The mass dependence of f_{NA} , which is proportional to $A_{\text{core}}^{-2/3}$, is that suggested^{7,8} for DCX in cases for which

there is no DIAT, i.e., on $T=0$ targets.

Recently another two-amplitude model has been proposed⁹ as arising from a description of the calcium isotopes in terms of the $\nu(f_{7/2})^n$ shell-model space with seniority zero. That result for the Ca isotopes has been further generalized¹⁰ to apply to DCX transitions between any $(f_{7/2})^n$ nuclei. In that framework,

$$\text{factor} = \frac{1}{(2j-1)(2T+3)(2T-1)} \left[(n+3)(2j+3-2n) + \frac{(n-2T)(n+2T+2)(6j+7)}{4(j+1)} \right]. \quad (5)$$

In addition to providing an expression for $d\sigma^{\text{DIAS}}/d\Omega_{\text{DCX}}$, this model also provides an expression for the cross section for transitions to the ground state (g.s.) of the final nucleus $d\sigma^{\text{g.s.}}/d\Omega_{\text{DCX}}$:

$$\frac{d\sigma^{\text{g.s.}}}{d\Omega_{\text{DCX}}} = \left| \frac{(2j+1)}{8(2j-1)(j+1)} \left[\frac{T(T-1)(n+2T+2)(n-2T+4)(4j+6-n-2T)(4j+4-n+2T)}{(2T-1)(2T+1)} \right]^{1/2} \times B \right|^2. \quad (6)$$

In these expressions T is the isospin of the target nucleus. The quantity n is the smaller of the number of particles or holes in the shell and j is the angular momentum of the shell being considered. For $(f_{7/2})^n$ nuclei, $j = \frac{7}{2}$ and n is the smaller of $A_{\text{tgt}} - 40$ and $56 - A_{\text{tgt}}$. The quantities A and B depend on pion kinetic energy, but at a given T_π they can be determined by fitting the experimental cross sections. References 9 and 10 do not address the question of the dependence of A and B on A_{tgt} .

In this paper we report differential cross sections for transitions to the DIAS at $T_\pi \sim 292$ MeV and $\theta_{\text{lab}} = 5^\circ$ on seven targets and limits for the nonanalog transition to the ground state on the four $T > 1$ targets. These measurements were performed at the Clinton P. Anderson Meson Physics Facility (LAMPF) using the EPICS channel and spectrometer in the configuration for small-angle DCX measurements.¹¹ Targets used included $^{30}\text{SiO}_2$, ^{34}S , $^{44}\text{CaCO}_3$, $^{50}\text{TiO}_2$, natural V metal, natural Cr metal and $^{52}\text{CrO}_2$, and ^{58}Ni metal. Figure 1 shows the spectra for the three $N=28$ targets measured in this work. Target thicknesses and enrichments are listed in Table I along with the measured cross sections. The data for ^{50}Ti and ^{52}Cr , for which there was a significant fraction of the other isotopes in the targets, have been corrected by estimates of the contribution of the other isotopes to the DIAS peak. This correction is necessary because the DIAS Q value is nearly the same for all the isotopes of a given Z , and these contributions are not resolved. These estimates were made by assuming that the $T=1$ ($T > 1$) DIAS cross sections are proportional to $A_{\text{tgt}}^{-7/3}$ ($A_{\text{tgt}}^{-10/3}$) and using the relative percentages of the different isotopes in the targets. The fraction of DIAS counts from the isotope of interest is 0.826 and 0.858 for the ^{50}Ti and ^{52}Cr targets, respectively. We estimate these numbers to be accurate to $\sim 1.5\%$ and these uncertainties have been included in the errors given in Table I for the ^{50}Ti and ^{52}Cr targets. Absolute normalizations were made by comparison to $^1\text{H}(\pi^+, \pi^+) ^1\text{H}$ scattering. We estimate the uncertainty in our absolute normalizations to be $\pm 5\%$.

$$\frac{d\sigma^{\text{DIAS}}}{d\Omega_{\text{DCX}}} = \frac{(N-Z)(N-Z-1)}{2} |A + \text{factor} \times B \times e^{i\psi}|^2, \quad (4)$$

where ψ is the relative phase between the two amplitudes and

Our new DIAS measurements, together with the previous data^{1,2,12-16} at $T_\pi \sim 292$ MeV and $\theta_{\text{lab}} = 5^\circ$ for $A_{\text{tgt}} \leq 60$, are displayed in Fig. 2. Also shown in Fig. 2 are the results of fitting the seven $T=1$ cross sections to an $A_{\text{tgt}}^{-7/3}$ dependence; of fitting all the displayed data and the ^{88}Sr (Ref. 17), ^{90}Zr (Ref. 17), ^{208}Pb (Ref. 18), and ^{209}Bi (Ref. 19) cross sections to an $A_{\text{tgt}}^{-10/3}$ dependence; and the results of fitting the displayed data to the FG two-amplitude model, Eq. (1). The results of the FG fit to the DIAS cross sections for $A \leq 58$ are given in Table II.

In Fig. 3 we display the data shown in Fig. 2 for $42 \leq A_{\text{tgt}} \leq 54$, along with the results of fitting the $(f_{7/2})^n$ DIAS data to Eq. (4) and the associated predictions for the other $T=1$ nuclei (^{46}Ti , ^{50}Cr , and ^{54}Fe) in this mass region. The results of the $(f_{7/2})^n$ fit are listed

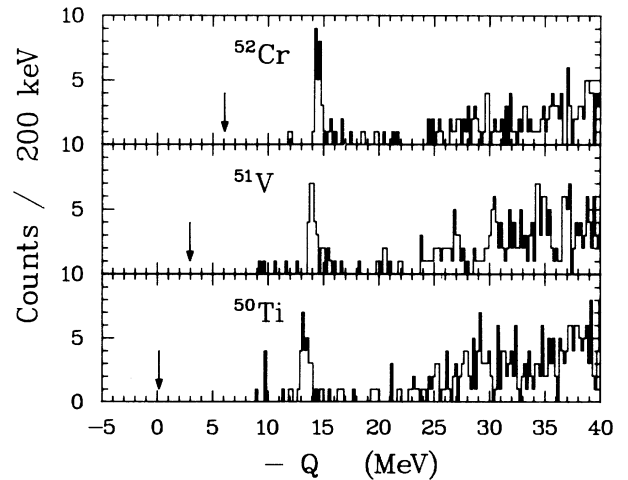


FIG. 1. Spectra obtained in this work for the (π^+, π^-) reaction on targets of ^{50}Ti , ^{51}V , and ^{52}Cr . The DIAS is clearly apparent. The arrows show the expected position of the residual ground state for each target.

TABLE I. New (π^+ , π^-) differential (lab) cross sections at $\theta_{\text{lab}}=5^\circ$ measured in this work.

Target isotope	T	$\frac{d\sigma}{d\Omega}$ (DIAS) ($\mu\text{b/sr}$)	$\frac{d\sigma}{d\Omega}$ (g.s.) ($\mu\text{b/sr}$)	ρx^a (mg/cm^2)	ρx_{total} (mg/cm^2)	Enrichment (%)
$^{30}\text{Si}^b$	1	0.703 ± 0.287		127	286	91.6
$^{34}\text{S}^b$	1	0.591 ± 0.143		255	255	94.3
$^{44}\text{Ca}^b$	2	0.637 ± 0.102	0.014 ± 0.014	422	1525	98.4
$^{50}\text{Ti}^c$	3	0.968 ± 0.201	≤ 0.066	72	191	67.5
$^{51}\text{V}^c$	$\frac{5}{2}$	0.766 ± 0.155	≤ 0.043	243	243	> 99
$^{52}\text{Cr}^c$	2	0.574 ± 0.111	≤ 0.028	303	390	88.7
$^{58}\text{Ni}^b$	1	0.154 ± 0.058^d		300	300	99.9
$^{58}\text{Ni}^c$	1	0.152 ± 0.033^d		1100	1100	99.9

^aThis is the ρx of the isotope of interest in the target.

^b $T_\pi \sim 292$ MeV.

^c $T_\pi \sim 290$ MeV.

^dAverage $(d\sigma/d\Omega)(^{58}\text{Ni}) = 0.152 \pm 0.029$ $\mu\text{b/sr}$ from this work; K. K. Seth *et al.*, Phys. Lett. **173B**, 397 (1986) reports $(d\sigma/d\Omega)(^{58}\text{Ni}) = 0.110 \pm 0.017$ $\mu\text{b/sr}$.

in Table III. Using the value of B ($0.440^{+0.084}_{-0.105}$) that results from this fit in Eq. (6), we obtain predictions for g.s. cross sections that are 5–20 times larger than the experimental values (see Table III). One also sees (Fig. 3) that this fit predicts cross sections for the other $T=1$ nuclei, ^{46}Ti , ^{50}Cr , and ^{54}Fe , that are significantly larger than the $A_{\text{tgt}}^{-7/3}$ curve.

If the DCX cross sections to the g.s. for the ($f_{7/2}$)ⁿ nuclei are fitted with Eq. (6) while the DIAS cross sections are simultaneously fitted with Eq. (4), we obtain a value of A (0.287 ± 0.011) that is very close to the value (0.276 ± 0.012) obtained from fitting only the DIAS cross sections. However, the ratio of B/A is 0.43 ± 0.08 as compared to the value $1.59^{+0.39}_{-0.43}$ from fitting only the

DIAS data. This ratio (0.43) is now consistent with the DCX reaction to the DIAS at 292 MeV being dominated by transitions through the isobaric analog state (IAS). The latter fit predicts that the ^{46}Ti , ^{50}Cr , and ^{54}Fe DIAS cross sections will be roughly proportional to $A_{\text{tgt}}^{-7/3}$ consistent with other $T=1$ nuclei, as opposed to the DIAS-only fit, which predicts cross sections much larger than the $A_{\text{tgt}}^{-7/3}$ dependence (see Fig. 3).

While the reduced χ^2 (2.44) for the fit with ground states is larger than that (0.13) from fitting the DIAS

TABLE II. Results^a of the Fortune-Gilman model [Eqs. (1)–(3)] fit to DIAS cross sections at $T_\pi=292$ MeV and $\theta_{\text{lab}}=5^\circ$.

Target	T	A_{core}	$\frac{d\sigma}{d\Omega_{\text{lab}}}$ ($\mu\text{b/sr}$)	$\frac{d\sigma}{d\Omega_{\text{calc}}}$ ($\mu\text{b/sr}$)	χ^2
$^{14}\text{C}^b$	1	16	4.610 ± 0.403	4.263	0.74
$^{18}\text{O}^c$	1	16	2.273 ± 0.118	2.319	0.15
$^{26}\text{Mg}^d$	1	28	1.000 ± 0.143	0.828	1.45
$^{30}\text{Si}^e$	1	28	0.703 ± 0.287	0.659	0.02
$^{34}\text{S}^e$	1	32	0.591 ± 0.143	0.501	0.39
$^{42}\text{Ca}^f$	1	40	0.404 ± 0.061	0.326	1.64
$^{44}\text{Ca}^e$	2	40	0.600 ± 0.096	0.699	1.06
$^{48}\text{Ca}^f$	4	40	1.746 ± 0.290	1.820	0.07
$^{48}\text{Ti}^f$	2	40	0.590 ± 0.103	0.584	0.00
$^{50}\text{Ti}^e$	3	40	0.968 ± 0.201	0.986	0.01
$^{51}\text{V}^e$	$\frac{5}{2}$	40	0.766 ± 0.155	0.707	0.14
$^{52}\text{Cr}^e$	2	40	0.574 ± 0.111	0.503	0.41
$^{56}\text{Fe}^g$	2	56	0.306 ± 0.051	0.359	1.07
$^{58}\text{Ni}^e$	1	56	0.152 ± 0.029	0.180	0.92

^aThis fit gives $\chi^2_{\text{total}} = 8.07$ with $f_{\text{NA}}(^{18}\text{O}) = 0.87^{+0.17}_{-0.21}$, $f_{\text{DIAS}}(^{18}\text{O}) = 1.19^{+0.20}_{-0.24}$, and $\phi = 86^\circ \pm 18^\circ$.

^bAverage of values from Ref. 2 and Ref. 14.

^cAverage of values from Ref. 12 and Ref. 15.

^dReference 12.

^eThis work.

^fReference 13.

^gAverage of values from Ref. 1 and Ref. 16.

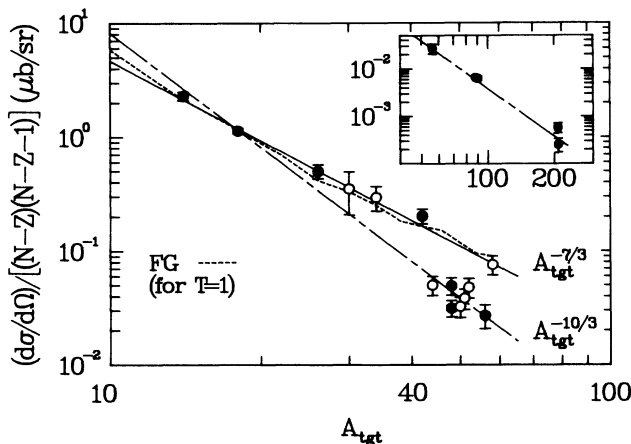


FIG. 2. $d\sigma/d\Omega/[(N-Z)(N-Z-1)]$ vs A_{tgt} for the DIAS for $A_{\text{tgt}} \leq 60$. The inset shows the data for $A_{\text{tgt}} \geq 56$. The solid line is $1006 \times A_{\text{tgt}}^{-7/3}$; the chain-dash line is $17615 \times A_{\text{tgt}}^{-10/3}$; the dash line is from the Fortune-Gilman model for the $T=1$ nuclei when all of the $A \leq 60$ data are fitted, see text for discussion. The open circles are from this work and the solid circles are previous data.

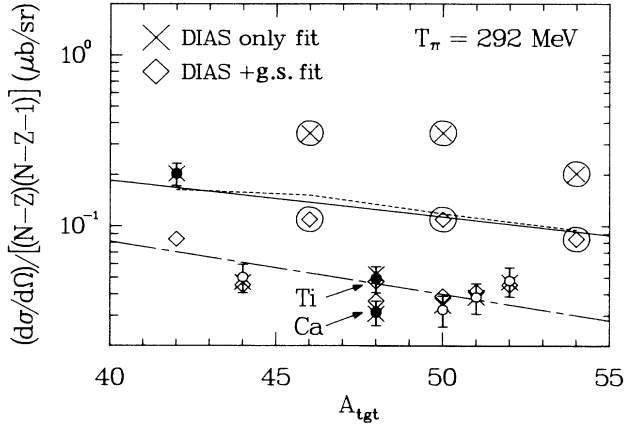


FIG. 3. $(d\sigma/d\Omega)/[(N-Z)(N-Z-1)]$ vs A_{tgt} for the DIAS transitions for $42 \leq A_{\text{tgt}} \leq 54$ [i.e., the region of the $(f_{7/2})^n$ shell]. The lines are the same as described for Fig. 2; the \times 's are the fit using the expressions given in Ref. 10 to fit the DIAS data only. The diamonds are from a fit that also includes the ground-state cross sections in addition to the DIAS cross sections. The circled \times 's and diamonds are predictions for the $T=1$ nuclei ^{46}Ti , ^{50}Cr , and ^{54}Fe from the respective fits.

data alone, most of the increase comes from the ^{42}Ca DIAS cross section, which is underpredicted by more than a factor of 2. From Eqs. (4)–(6) and Table III one sees that the sensitivity to the B term is greatest for the g.s. cross sections (for which A is absent) and then to the $T=1$ DIAS cross sections, for which the coefficient

of B is large, and finally to the $T > 1$ DIAS cross sections. The ^{42}Ca DIAS cross section may be enhanced by core polarization effects, and consequently the seniority-zero model may underpredict this cross section. If the ^{42}Ca cross section were so enhanced, this would cause the DIAS only $(f_{7/2})^n$ fit to give an incorrect value of B since without the g.s. data it is most sensitive to the $T=1$ data, and ^{42}Ca is currently the only $T=1$ data point in the $(f_{7/2})^n$ data set. The poor agreement for ^{42}Ca could also be partially due to the assumption that A and B have no A_{tgt} dependence.

It should be noted that, for the two two-amplitude models discussed here, one term of each is very similar in appearance. These are f_{DIAS} of the FG model [Eq. (1)] and the A term in Eq. (4), which is attributed^{9,10} to monopole transitions through intermediate nuclear states. If we multiply $f_{\text{DIAS}}(^{18}\text{O}) = 1.19_{-0.24}^{+0.20}$ by $(\frac{18}{42})^{5/3}$ to scale it to ^{42}Ca , we obtain $0.290_{-0.058}^{+0.049}$, which is in agreement with the value of A , 0.276 ± 0.012 (without g.s. fit) or 0.287 ± 0.011 (with g.s. fit). The second amplitude in the two models appears to have different origins. In the FG model it is due to nonanalog transitions involving the core while in the seniority-zero model it is due to higher-multipolarity nonanalog transitions^{9,10} purely within the valence nucleons. Thus the coefficients of the second amplitude from the two models cannot be compared.

In conclusion, we report seven new differential cross sections for double charge exchange to the double isobaric analog state and report limits for four nonanalog transitions to the ground state at $T_\pi \sim 292$ MeV and $\theta_{\text{lab}} = 5^\circ$. Three of the new DIAS measurements are for $T=1$ targets and further emphasize that if the $T=1$ nu-

TABLE III. Results of fitting the $(f_{7/2})^n$ expressions [Eqs. (4)–(6)] to DCX cross sections.

Transition	$\frac{d\sigma}{d\Omega_{\text{exp}}}$ ($\mu\text{b/sr}$)	DIAS only fit ^a		DIAS + g.s. fit ^b		Factor ^c
		$\frac{d\sigma}{d\Omega_{\text{calc}}}$ ($\mu\text{b/sr}$)	χ^2	$\frac{d\sigma}{d\Omega_{\text{calc}}}$ ($\mu\text{b/sr}$)	χ^2	
$^{42}\text{Ca} \rightarrow ^{42}\text{Ti}(\text{g.s.}, \text{DIAS})^{\text{d}}$	0.404 ± 0.061	0.404	0.00	0.167	15.04	1.000
$^{44}\text{Ca} \rightarrow ^{44}\text{Ti}(\text{DIAS})$	0.600 ± 0.096	0.562	0.16	0.542	0.37	0.1111
$^{48}\text{Ca} \rightarrow ^{44}\text{Ti}(\text{DIAS})^{\text{d}}$	1.746 ± 0.290	1.714	0.01	2.033	0.98	-0.1429
$^{48}\text{Ti} \rightarrow ^{48}\text{Cr}(\text{DIAS})^{\text{d}}$	0.590 ± 0.103	0.626	0.12	0.567	0.05	0.1675
$^{50}\text{Ti} \rightarrow ^{50}\text{Cr}(\text{DIAS})$	0.968 ± 0.201	1.025	0.08	1.165	0.97	-0.0667
$^{52}\text{Cr} \rightarrow ^{52}\text{Fe}(\text{DIAS})$	0.574 ± 0.111	0.562	0.01	0.542	0.08	0.1111
$^{44}\text{Ca} \rightarrow ^{44}\text{Ti}(\text{g.s.})$	0.014 ± 0.014	0.306		0.024	0.47	1.2571
$^{48}\text{Ca} \rightarrow ^{48}\text{Ti}(\text{g.s.})^{\text{d}}$	≤ 0.051	0.262		0.020	0.16	1.1638
$^{48}\text{Ti} \rightarrow ^{48}\text{Cr}(\text{g.s.})^{\text{d}}$	0.025 ± 0.013	0.444		0.034	0.51	1.5147
$^{50}\text{Ti} \rightarrow ^{50}\text{Cr}(\text{g.s.})$	≤ 0.066	0.367		0.028	0.18	1.3771
$^{52}\text{Cr} \rightarrow ^{52}\text{Fe}(\text{g.s.})$	≤ 0.028	0.306		0.024	0.71	1.2571
$^{51}\text{V} \rightarrow ^{51}\text{Mn}(\text{DIAS})^{\text{e}}$	0.766 ± 0.155	0.764		0.823		0.0000
$^{51}\text{V} \rightarrow ^{51}\text{Mn}(\text{g.s.})^{\text{e}}$	≤ 0.043	0.358		0.028		1.3608

^aThis fit gives $A = 0.276 \pm 0.012$, $B = 0.440_{-0.105}^{+0.084}$, $\psi = 56^\circ \pm 34^\circ$, and $\chi^2_{\text{total}} = 0.38$.

^bThis fit gives $A = 0.287 \pm 0.011$, $B = 0.122_{-0.018}^{+0.016}$, $\psi = 0^\circ \pm 23^\circ$, and $\chi^2_{\text{total}} = 19.52$.

^cFor the DIAS transitions this is the value of Eq. (5) and for the g.s. transitions this is the value that multiplies B in Eq. (6).

^dData from Ref. 13.

^eWhile the calculated values are from Eqs. (4) and (6), these transitions were not included in the fit because the model is for $0^+ \rightarrow 0^+$ transitions and this is a $J^\pi = \frac{7}{2}^-$ target.

clei are considered alone the A_{tgt} dependence is $A_{\text{tgt}}^{-7/3}$. The FG two-amplitude model reproduces the data with the expected $A_{\text{tgt}}^{-10/3}$ dependence for the DIAT amplitude. A new model based on the seniority-zero shell model is used to compare DIAS cross sections for the $(f_{7/2})^n$ nuclei, where we report new measurements for DIAS cross sections and limits for the cross sections to the g.s. on four $T > 1$ targets. If only the $(f_{7/2})^n$ DIAS cross sections are fitted, then the predictions for other $T = 1$ DIAS cross sections are larger than predicted by the $A_{\text{tgt}}^{-7/3}$ fit. If the g.s. cross sections are also included in the fit then the DIAS cross sections are equally well

fitted, excluding ^{42}Ca , and the heavier $T = 1$ $(f_{7/2})^n$ cross section predictions lie near the $A_{\text{tgt}}^{-7/3}$ curve. While the DCX cross sections to ground states are limited in number, this work emphasizes the fact that such measurements are necessary and complement DIAS measurements.

This work was supported by the National Science Foundation, the U.S. Department of Energy, and the Robert A. Welch Foundation.

*Permanent address: Institute of Atomic Energy, Beijing, Peoples Republic of China.

†Present address: Argonne National Laboratory, Argonne, Illinois 60439.

‡Permanent address: Ben-Gurion University of The Negev, Beer-Sheva, Israel.

¹R. Gilman, H. T. Fortune, J. D. Zumbro, C. M. Laymon, G. R. Burleson, J. A. Faucett, W. B. Cottingame, C. L. Morris, P. A. Seidl, C. F. Moore, L. C. Bland, R. R. Kiziah, S. Mordechai, K. S. Dhuga, Phys. Rev. C **35**, 1334 (1987).

²P. A. Seidl, M. D. Brown, R. R. Kiziah, C. F. Moore, H. Baer, C. L. Morris, G. R. Burleson, W. B. Cottingame, S. J. Greene, L. C. Bland, R. Gilman, and H. T. Fortune, Phys. Rev. C **30**, 973 (1984).

³H. T. Fortune and R. Gilman, Phys. Rev. C **33**, 2171 (1986).

⁴S. J. Greene, D. B. Holtkamp, W. B. Cottingame, C. F. Moore, G. R. Burleson, C. L. Morris, H. A. Thiessen, and H. T. Fortune, Phys. Rev. C **25**, 924 (1982).

⁵R. Gilman, L. C. Bland, P. A. Seidl, C. F. Moore, C. L. Morris, S. J. Greene, H. T. Fortune, Nucl. Phys. **A432**, 610 (1985).

⁶M. B. Johnson, Phys. Rev. C **22**, 192 (1980).

⁷C. L. Morris, H. T. Fortune, L. C. Bland, R. Gilman, S. J. Greene, W. B. Cottingame, D. B. Holtkamp, G. R. Burleson, and C. F. Moore, Phys. Rev. C **25**, 3218 (1982).

⁸L. C. Bland, R. Gilman, M. Carchidi, K. Dhuga, C. L. Morris, H. T. Fortune, S. J. Greene, P. A. Seidl, and C. F. Moore, Phys. Lett. **128B**, 157 (1983).

⁹N. Auerbach, W. R. Gibbs, and E. Piasezky, Phys. Rev. Lett. (in press).

¹⁰J. N. Ginocchio, W. R. Gibbs, N. Auerbach, and W. B. Kauffman (unpublished); and private communication.

¹¹S. J. Greene, W. J. Braithwaite, D. B. Holtkamp, W. B. Cot-

tingame, C. F. Moore, C. L. Morris, H. A. Thiessen, G. R. Burleson, and G. S. Blanpied, Phys. Lett. **88B**, 62 (1979).

¹²S. J. Greene, W. J. Braithwaite, D. B. Holtkamp, W. B. Cottingame, C. F. Moore, G. R. Burleson, G. S. Blanpied, A. J. Viescas, G. H. Daw, C. L. Morris, and H. A. Thiessen, Phys. Rev. C **25**, 927 (1982); and S. J. Greene, Ph.D. thesis, University of Texas, Los Alamos Report LA-8891-T (1981).

¹³M. Kaletka, Ph.D. thesis, Northwestern University, Los Alamos Report LA-9947-T (1983); and K. K. Seth, M. Kaletka, S. Iversen, A. Saha, D. Barlow, D. Smith, and L. C. Liu, Phys. Rev. Lett. **52**, 894 (1984).

¹⁴R. Gilman, H. T. Fortune, J. D. Zumbro, P. A. Seidl, C. F. Moore, C. L. Morris, J. A. Faucett, G. R. Burleson, S. Mordechai, K. S. Dhuga, Phys. Rev. C **33**, 1082 (1986).

¹⁵P. A. Seidl, C. F. Moore, S. Mordechai, R. Gilman, K. S. Dhuga, H. T. Fortune, J. D. Zumbro, C. L. Morris, J. A. Faucett, and G. R. Burleson, Phys. Lett. **154B**, 255 (1985).

¹⁶P. A. Seidl, R. R. Kiziah, M. K. Brown, C. F. Moore, C. L. Morris, H. Baer, S. J. Greene, G. R. Burleson, W. B. Cottingame, L. C. Bland, R. Gilman, and H. T. Fortune, Phys. Rev. Lett. **50**, 1106 (1983).

¹⁷K. K. Seth, M. Kaletka, D. Barlow, D. Kielczewska, A. Saha, L. Casey, D. Godman, R. Seth, and J. Stuart, Phys. Lett. **155B**, 339 (1985).

¹⁸C. L. Morris, S. J. Greene, R. Gilman, H. T. Fortune, J. D. Zumbro, J. A. Faucett, G. R. Burleson, K. S. Dhuga, P. A. Seidl, S. Mordechai, and C. F. Moore, Phys. Rev. Lett. **54**, 775 (1985).

¹⁹C. L. Morris, H. A. Thiessen, W. J. Braithwaite, W. B. Cottingame, S. J. Greene, D. B. Holtkamp, I. B. Moore, C. F. Moore, G. R. Burleson, G. S. Blanpied, G. H. Daw, and A. J. Viescas, Phys. Rev. Lett. **45**, 1233 (1980).